Physics Letters B 775 (2017) 290–296

Contents lists available at ScienceDirect

Physics Letters B

www.elsevier.com/locate/physletb

Degenerate vacua to vacuumless model and kink–antikink collisions

F.C. Simas [a], Adalto R. Gomes [b,*], K.Z. Nobrega [c]

[a] Centro de Ciências Agrárias e Ambientais-CCAA, Universidade Federal do Maranhão (UFMA), 65500-000, Chapadinha, Maranhão, Brazil
[b] Departamento de Física, Universidade Federal do Maranhão (UFMA), Campus Universitário do Bacanga, 65085-580, São Luís, Maranhão, Brazil
[c] Departamento de Eletro-Eletrônica, Instituto Federal de Educação, Ciência e Tecnologia do Maranhão (IFMA), Campus Monte Castelo, 65030-005, São Luís, Maranhão, Brazil

ARTICLE INFO

Article history:
Received 6 June 2017
Received in revised form 5 September 2017
Accepted 7 November 2017
Available online 11 November 2017
Editor: M. Cvetič

ABSTRACT

In this work we investigate a Z_2 symmetric model of one scalar field ϕ in $(1,1)$ dimension. The model is characterized by a continuous transition from a potential $V(\phi)$ with two vacua to the vacuumless case. The model has kink and antikink solutions that minimize energy. Stability analysis is described by a Schrödinger-like equation with a potential that transits from a volcano-shape with no vibrational states (in the case of vacuumless limit) to a smooth valley with one vibrational state. We are interested in the structure of two-bounce windows present in kink–antikink scattering processes. The standard mechanism of Campbell–Schonfeld–Wingate (CSW) requires the presence of one vibrational state for the occurrence of two-bounce windows. We report that the effect of increasing the separation of vacua from the potential $V(\phi)$ has the consequence of trading some of the first two-bounce windows predicted by the CSW mechanism by false two-bounce windows. Another consequence is the appearance of false two-bounce windows of zero-order.

1. Introduction

Solitary waves are solutions from nonlinear physics characterized by the very special property of localized density energy that can freely propagate without distortion in their form. The realization of solitary waves in nature is now amply recognizable, with interesting effects in solid state and atomic physics [1].

The simplest solitary wave is described by the $(1,1)$ dimensional kink. Embedded in higher dimensions, the kinks generate domain walls or more generally p-branes in scenarios with extra dimensions. Brane collisions were considered as one possibility for generating the big bang, as in cyclic universe scenarios [2–4]. In particular, Refs. [3,4] considered particle production at the brane collision. For this, the simplest scenario of two domain walls in 5D Minkowski spacetime was considered. In the context of bubble collisions in the primordial universe, in some limit the effect of gravitational interaction between the bubbles can be negligible and the process of collisions can be described by kink–antikink in an effective $(1,1)$ dimensional model [5–7]. In this way the collision of nearly planar walls is a necessary step in understanding the full nonlinear dynamics of collisions between pairs of bubbles nucleating in false vacuum [8].

Usually kink models are constructed starting from a Lagrangian density

$$\mathcal{L} = \frac{1}{2}\partial_\mu\phi\partial^\mu\phi - V(\phi), \tag{1}$$

where the ϕ is a real scalar field and a potential $V(\phi)$ with minima at non-zero values of ϕ that suffers a spontaneous symmetry breaking. The equation of motion for the field $\phi(x,t)$ is given by

$$\phi_{tt} - \phi_{xx} + V_\phi = 0, \tag{2}$$

where we use the compact notation $V_\phi \equiv dV/d\phi$ and the like (similarly for higher-order derivatives, $V_{\phi\phi} \equiv d^2V/d\phi^2$). If we can write the potential in terms of the superpotential $V(\phi) = \frac{1}{2}W_\phi^2$, static configurations obeys one of the two first-order ordinary differential equations

$$\frac{d\phi}{dx} = \pm W_\phi. \tag{3}$$

The defects formed with this prescription minimize energy and are known as BPS defects [9,10].

Stability analysis considers small fluctuations

$$\Phi(x,t) = \phi(x) + \eta(x)\cos(\omega t), \tag{4}$$

* Corresponding author.
E-mail addresses: simasfc@gmail.com (F.C. Simas), argomes.ufma@gmail.com (A.R. Gomes), bzuza1@yahoo.com.br (K.Z. Nobrega).

https://doi.org/10.1016/j.physletb.2017.11.013

resulting in a Schrödinger-like equation

$$-\frac{d^2\eta}{dx^2} + V_{sch}(x)\eta = \omega^2\eta \tag{5}$$

with

$$V_{sch}(x) = V_{\phi\phi}(\phi(x)). \tag{6}$$

As one knows [11], this equation is factorizable, since it can be written as

$$S_{\pm}^{\dagger} S_{\pm}\eta = \omega^2\eta \tag{7}$$

with

$$S_{\pm} = -\frac{d}{dx} \pm W_{\phi\phi}, \tag{8}$$

which forbids the existence of tachyonic modes. Zero-mode exist, corresponding to a translational degree of freedom of the kink/antikink, and is given by

$$\eta_0 = C W_{\phi}, \tag{9}$$

with C a normalization constant.

Nonintegrable models like those considered here have the scattering process with a very rich character. The archetype model is the ϕ^4, where the main aspects were studied in deep (see for instance refs. [12–15]). There one knows that large initial velocities $v > v_{crit}$ lead to a simple scattering process where the kink–antikink pair encounter and after a single contact recede from themselves. This is called a 1-bounce process. Small initial velocities lead to the formation of a bound kink–antikink state called a bion that radiates continuously until being completely annihilated. Near to the frontier region bion/1-bounce, with velocities $v \lesssim v_{crit}$ it can occur the formation of two-bounce windows that accumulate toward $v = v_{crit}$ with smaller and smaller widths. At the edges of each two-bounce window another system of three-bounce windows can be found. This substructure is verified for even higher levels of bounce windows in a fractal structure [14]. Several models of kinks can be found in the recent literature, focusing on different aspects of structure and scattering dynamics from kinks [16–24].

Stability analysis of the kink leads to a Schrödinger-like equation where the presence of zero-mode is related to the translational invariance of the kink (invariance under Lorentz boosts). Usually one interprets the presence of non-null, bound states as vibrational states. In the standard Campbell–Schonfeld–Wingate (CSW) mechanism, a resonant exchange of energy between the translational and vibrational modes is responsible for the structure of two-bounce windows [13]. As far as we know there are two exceptions to this scenario: i) despite the absence of vibrational mode in the perturbation of a kink, considering the effect of collective antikink–kink structure, it was explained the reason for the occurrence of two-bounce windows in the ϕ^6 model [16]; ii) the presence of more that one vibrational state can in some circumstances destroy the two-bounce structure [22].

In this work we are interested in studying the effect of the separation of the vacua of the potential $V(\phi)$ in the process of kink–antikink collision, focusing mainly on the appearance and structure of two-bounce windows. In the Sect. 2 we will investigate a model with unusual scattering properties that can also contribute to an understanding of the mechanism of formation of two-bounce windows. In the Sect. 3 we present the numerical analysis of the kink–antikink scattering process. Our main conclusions are reported in the Sect. 4.

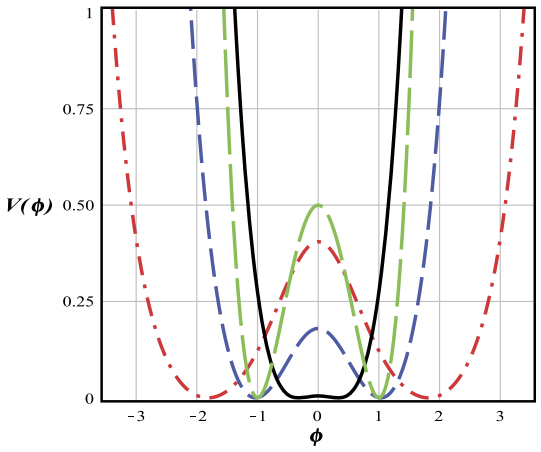

Fig. 1. Potential $V(\phi)$. The figures are for fixed $A = 0.1$ (red dash-dotted), $A = 0.4$ (blue dash), $A = 0.9$ (black line). Here it is also representing the potential for the ϕ^4 model (long-dashed green).

2. The model

An exception of the known mechanism for constructing kinks includes the so called vacuumless defects which are constructed in models with a potential that has a local maximum but no minima. One example is the model proposed by Cho and Vilenkin [25]:

$$V(\phi) = \mathrm{sech}^2(\phi). \tag{10}$$

Potentials of this type appear also in non-perturbative effects in supersymmetric gauge theories [26,27]. The equation of motion for the scalar field has the solution

$$\phi(x) = \sinh^{-1}(\sqrt{2}x) \tag{11}$$

which has finite energy.

Static solutions for this model where further studied both in their gravitational aspects in $(3,1)$ dimensions [28] and concerning to their topological structure and trapping of fields in $(1,1)$ dimensions [29]. More recently, Dutra and Faria Jr [30] considered an extension described by the potential

$$V(\phi) = \frac{1}{2}\Big(A\cosh(\phi) - \mathrm{sech}(\phi)\Big)^2. \tag{12}$$

Fig. 1 shows plots of $V(\phi)$ for several values of $0 < A < 1$, where there is the presence of two symmetric minima (due to the Z_2 symmetry) and a local maximum at $\phi = 0$. When A is reduced, the vacua are located at larger values of $|\phi|$ and the local maximum grows. The vacuumless potential from Cho and Vilenkin is recovered for $A \to 0$. Only for comparison, we plot the potential for the ϕ^4 model, showing that for the same vacua ($\phi = \pm 1$), the local maxima of the ϕ^4 potential is higher.

Static solutions for the scalar field are [30]

$$\phi_K^{(S)}(x) = \sinh^{-1}\left(\sqrt{\frac{1-A}{A}}\tanh\left(\sqrt{A(1-A)}x\right)\right), \tag{13}$$

for kink and $\phi_{\bar{K}}^{(S)}(x) = -\phi_K^{(S)}(x)$ for antikink. The vacua of the model are described by [30]

$$\phi(x \to \pm\infty) = \pm\cosh^{-1}\left(\sqrt{\frac{1}{A}}\right), \tag{14}$$

and the energy density is given by [30]

$$\rho(x) = \frac{(1-A)^2\cosh^{-4}(\sqrt{A(1-A)}x)}{1 + (1/A - 1)\tanh^2(\sqrt{A(1-A)}x)}. \tag{15}$$

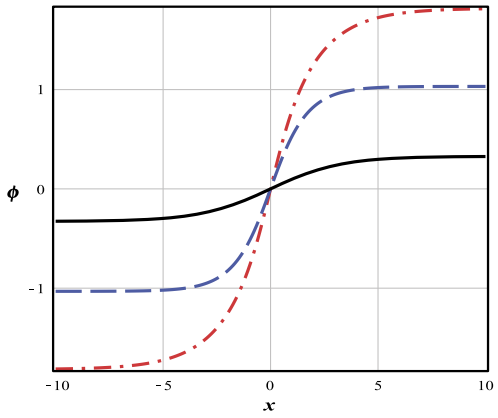

Fig. 2. Field configurations $\phi(x)$. The figures are for fixed $A = 0.1$ (red dash-dotted), $A = 0.4$ (blue dash), $A = 0.9$ (black line).

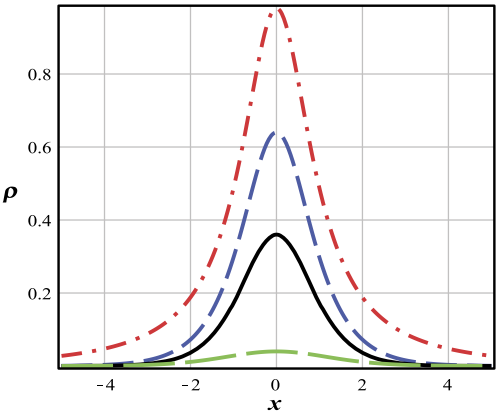

Fig. 3. The energy density $\rho(x)$. The figures are for fixed $A = 0.01$ (red dash-dot), $A = 0.2$ (blue dashed), $A = 0.4$ (black line) and $A = 0.8$ (green long-dash).

Fig. 2 depicts some plots of $\phi(x)$ for several values of A. In the limit of a vacuumless model $A = 0$ the maximum of $\phi(x)$ goes to infinity. Despite this, the energy density is a localized function of x even close to the vacuumless limit, as can be seen in Fig. 3

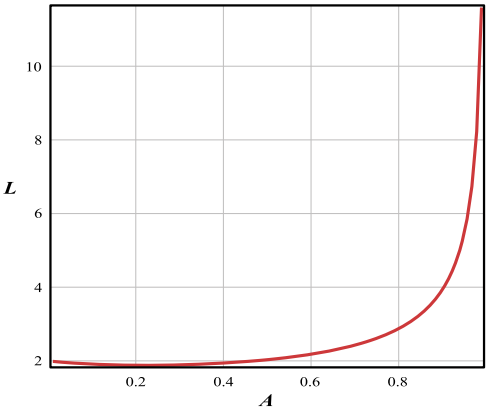

Fig. 4. Kink width L as a function of A. Note the minimum around $A \simeq 0.22$. See also Fig. 5.

(for more details see ref. [30]). One can define the kink width L of the defect as the full width at half maximum (FWHM) of the corresponding peak of energy density. The influence of A on the kink width is given in Fig. 4. From the figure we see a minimum around $A_* \simeq 0.22$, with an almost constant width for $0 < A < 2A_*$ whereas for $A > A_*$ the increasing in the separation of the vacua turns the kinks with bigger widths. Fig. 5 shows a diagram useful for comparing the influence of A on different characteristics of the model presented further in this paper.

Figs. 6a–6b depict some plots of the Schrödinger-like potential V_{sch} of perturbations for several values of A. When $A \to 0$, we have V_{sch} with a volcano-shape with a deep minimum. The increasing of A up to $A = 0.5$ (see Fig. 6a) reduces the depth of the minimum and increases the asymptotic maximum of the potential. For $0.5 < A < 1$ (see Fig. 6b) the asymptotic maximum is reduced, whereas the depth of the minimum continues to decrease. Then in this region, we have a continuous reduction of the difference between minimum and maximum of the potential, with a broader shape.

With this potential the occurrence of bound states was investigated numerically. For all values of $0 < A < 1$ there is always a zero-mode. The structure of vibrational states is summarized in

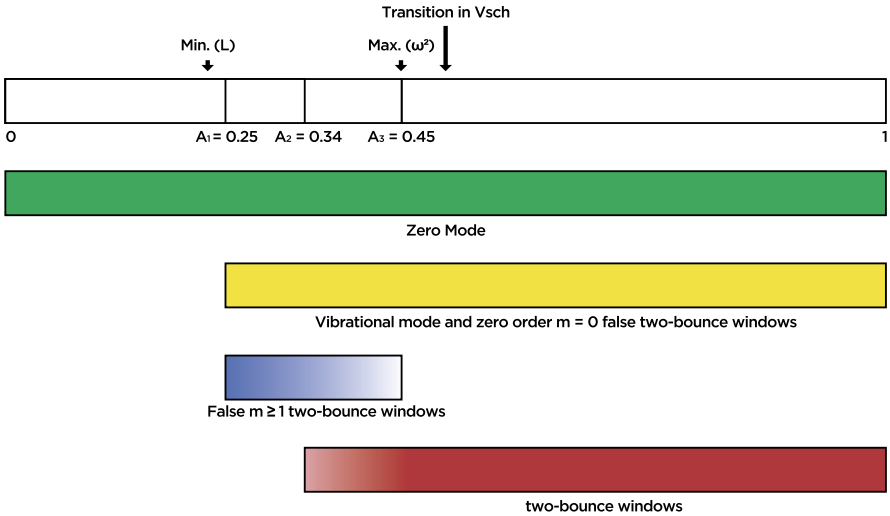

Fig. 5. Diagram for $0 < A < 1$ showing the main characteristics of the model: i) minimum value of kink width L for $A = 0.22$; ii) stability analysis showing the presence of zero-mode for $0 < A < 1$ (green); iii) stability analysis with a vibrational mode and presence of zero-order $m = 0$ false two-bounce windows for $A_1 < A < 1$ (yellow); iv) maximum of squared frequency ω^2 of the vibrational states for $A = 0.44$; v) Transition of V_{sch} at $A = 0.5$; vi) presence of $m \geq 1$ false two-bounce windows for $A_1 < A < A_3$ (brighter blue color for stronger effects); vii) Presence of the complete structure of two-bounce windows for $A_3 < A < 1$ (red); viii) suppression of two-bounce windows for $A_2 < A < A_3$ (brighter red color for stronger effects). (For interpretation of the references to color in this figure legend, the reader is referred to the web version of this article.)

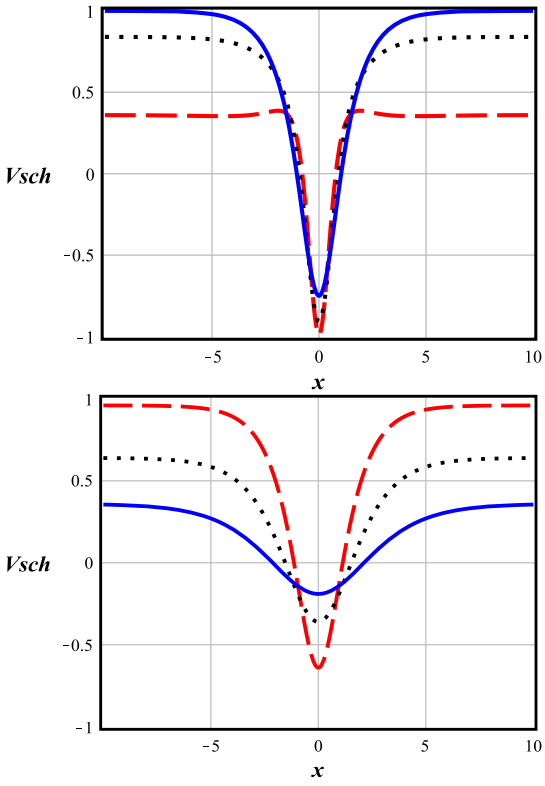

Fig. 6. Schrödinger-like potential $V_{sch}(x)$. (a) (upper) The figures are for fixed $A = 0.1$ (red dash), $A = 0.3$ (black dotted), $A = 0.5$ (blue solid). (b) (bottom) The figures are for fixed $A = 0.6$ (red dash), $A = 0.8$ (black dotted), $A = 0.9$ (blue solid). Note that there is a transition around $A \sim 0.5$. See also Fig. 5.

Table 1
Structure of vibrational states with A. Second column gives squared frequency of the first vibrational state. Third column is the order m of first observed two-bounce window – i.e., the number of oscillations of $\phi(0,t)$ between bounces (see Sec. 3).

A	ω^2 for vibrational state	order m of first two-bounce window
0.1	–	–
0.2	–	–
0.3	0.8256	–
0.4	0.9006	3
0.5	0.8946	1
0.6	0.8223	1
0.7	0.6920	1
0.8	0.5093	1
0.9	0.2777	1
0.98	0.0609	1

Table 1 and Fig. 7. There one can see that for $0 < A \lesssim 0.256$ only a zero-mode appears, with no vibrational states. In particular, case $A = 0$, the true vacuumless case, which has a volcano-shape potential V_{sch}, possibly has resonances. However, since the existence of resonances is not relevant for the formation of two-bounces we will not elaborate on this. In the Fig. 7 we can see some plots of squared frequencies ω^2 as a function of the parameter A. For $0.257 \lesssim A \lesssim 1$ we have the presence of one vibrational mode – see also Fig. 5). Note also that the frequency squared of the vibrational mode grows with A to a maximum for $A \sim 0.44$, reducing monotonically for larger values of A and going to zero for $A \to 1$.

3. Numerical results

In this section we present our main results of the kink–antikink scattering process. We are interested in the effect of the separation of vacua of $V(\phi)$ given by Eq. (12) for intermediate initial

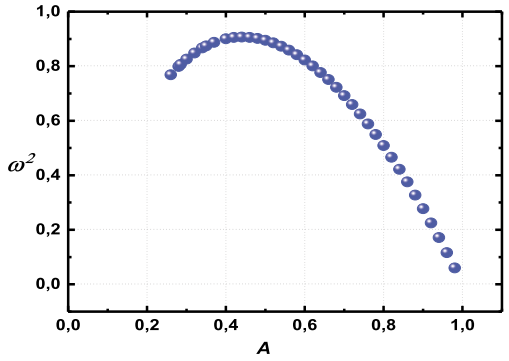

Fig. 7. Squared frequency ω^2 for the vibrational state as a function of A. The curve has a maximum at $A = 0.44$. See also Fig. 5.

velocities, where it is verified the presence of bounce windows. In particular, we focus on the structure of two-bounce windows and their relation with the structure of vibrational states.

We considered a symmetric kink–antikink collision. Initial conditions are given by sufficiently distant defects described by boosting free solutions:

$$\phi(x,0) = \phi_K(x+x_0,0) + \phi_{\bar{K}}(x-x_0,0) - \cosh^{-1}\left(\sqrt{\frac{1}{A}}\right), \tag{16}$$

$$\dot{\phi}(x,0) = \dot{\phi}_K(x+x_0,0) + \dot{\phi}_{\bar{K}}(x-x_0,0). \tag{17}$$

Here $\phi_K(x,t) = \phi_K^{(S)}(\gamma(x-vt))$ and $\phi_{\bar{K}}(x,t) = \phi_{\bar{K}}^{(S)}(\gamma(x+vt))$ means free kink and antikink solution, respectively. Here $\gamma = (1-v^2)^{-1/2}$ and we fixed $x_0 = 15$ as the initial kink position, i.e., the kink solution centered at $-x_0$ and the antikink at x_0. For solving the equation of motion given by Eq. (2) we used a pseudospectral method on a grid with 2048 nodes with periodic boundary conditions for ϕ and $\dot{\phi}$. Also, we set the grid boundary at $x_{max} = 200$.

In Figs. 8a–c we show some plots of the final velocity as a function of initial velocity. For large velocities ($v > v_{crit}$) we have the inelastic scattering corresponding to 1-bounce. For $v < v_{crit}$, we have two possibilities: i) the final velocity is zero, indicating the trapping of the kink–antikink pair into an oscillatory state – the bion; ii) depending on the value of A, there are regions of non-null final velocities with variable widths in between bion states – these correspond to bounce windows. Fig. 8a, for $A = 0.2$, has the critical velocity v_{crit} close to 1, showing that the scattering processes lead almost always to bion states with just a small interval in initial velocities leading to collisions with 1-bounce. This plot shows us the absence of two-bounce windows. On the other hand, the Figs. 8b and 8c, respectively, for $A = 0.6$ and $A = 0.9$, show the presence of two-bounce windows with smaller v_{crit}. This is made clearer in Fig. 9. There one can see how v_{crit} decreases with A. This indicates that potentials with degenerated vacua with smaller $|\phi|$ favor the enlargement of the 1-bounce region. In particular, in the limit of a vacuumless model ($A \to 0$) only bion states are produced.

As we saw, small values of A ($0 < A \lesssim A_1$, with $A_1 = 0.25$) correspond to cases without vibrational mode (see Table 1 and Fig. 7), where there is no two-bounce windows at all, in accord with what expected from the standard CSW mechanism [13]. There is an interval $A_1 < A \lesssim A_2$, with $A_2 = 0.34$ where, despite the presence of a vibrational mode, there are no two-bounce windows. The two-bounce windows are present for larger values of A ($A_2 \lesssim A < 1$). In the Figs. 10a–10d we plot the behavior of the times of first, second and third kink–antikink collisions as a function of initial velocity

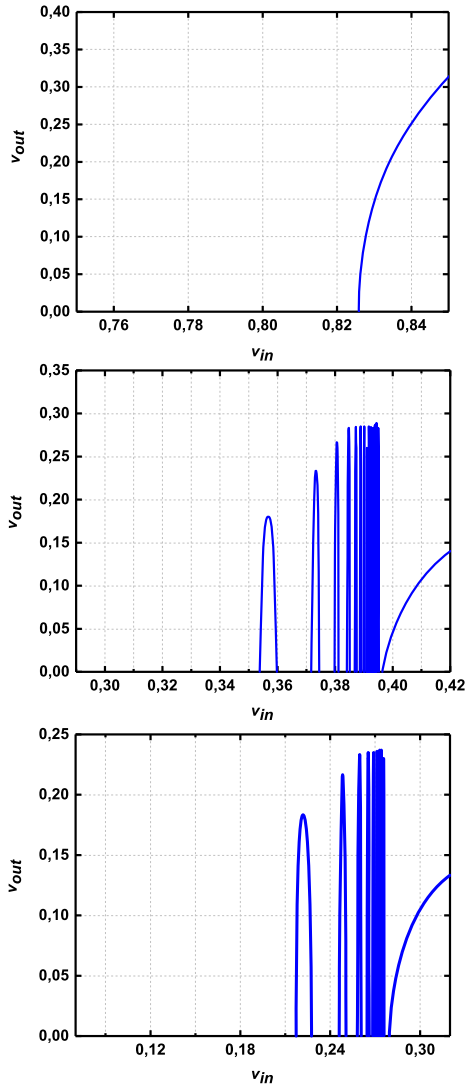

Fig. 8. The output (final) kink velocity after a $K\bar{K}$ collision as a function of input (initial) velocities for a) $A = 0.2$, b) $A = 0.6$ and c) $A = 0.9$.

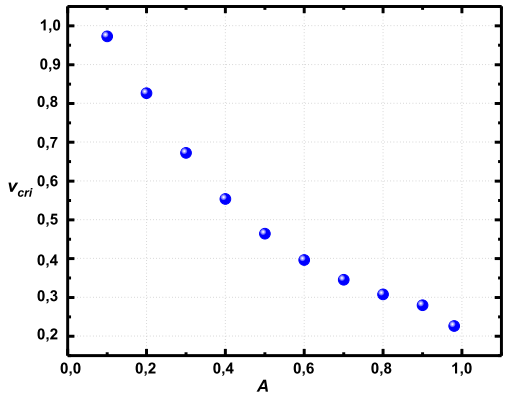

Fig. 9. Critical velocity as a function of A.

for fixed values of A. As shown in Table 1 and Fig. 7, these cases correspond to examples with one vibrational mode. For $A = 0.9$ (Fig. 10d), the presence of a vibrational mode induces the appearance of two-bounce windows, recognized in the figure by regions where there is a divergence in the times corresponding to a third collision.

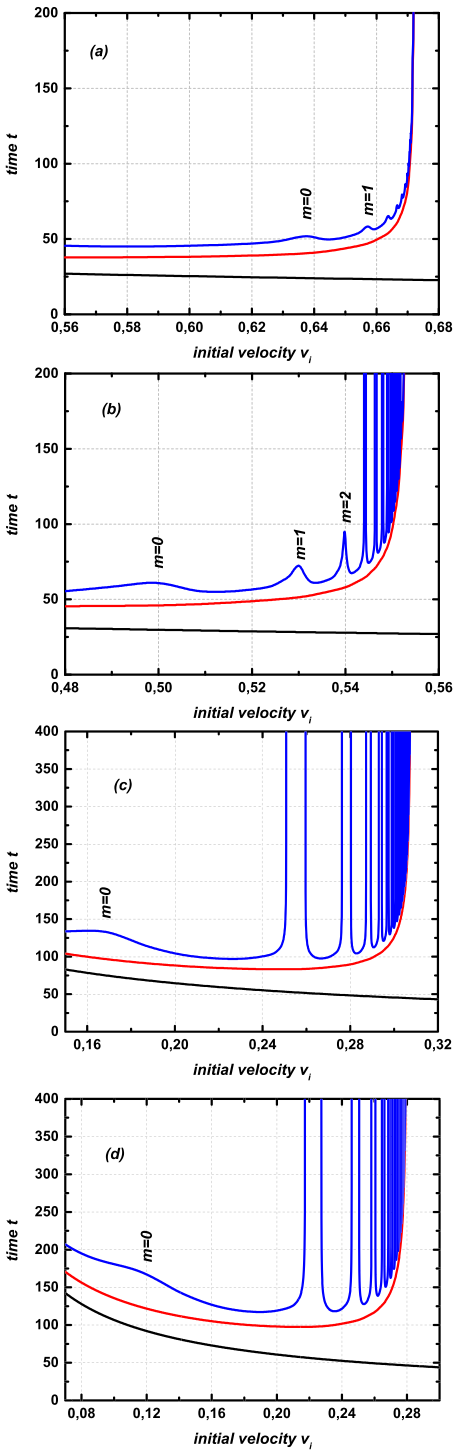

Fig. 10. Times to the first (black), second (red) and third (blue) kink–antikink collisions as a function of initial velocity v_i for a) $A = 0.3$, b) $A = 0.4$, c) $A = 0.8$, d) $A = 0.9$. Some peaks include also the number m of oscillations between bounces for the observed false two-bounce windows. (For interpretation of the references to color in this figure legend, the reader is referred to the web version of this article.)

We note also the presence of a first smooth peak unexpected from CSW mechanism. This is called a zero-order false two-bounce windows, and as far as we know, were first observed in the context of ϕ^6 model [16]. Now, if we slowly reduce the value of A back to zero, the structure of zero-order false two-bounce windows is enlarged, reducing their height until finally disappearing for $A \lesssim 0.25$ (see diagram of Fig. 5).

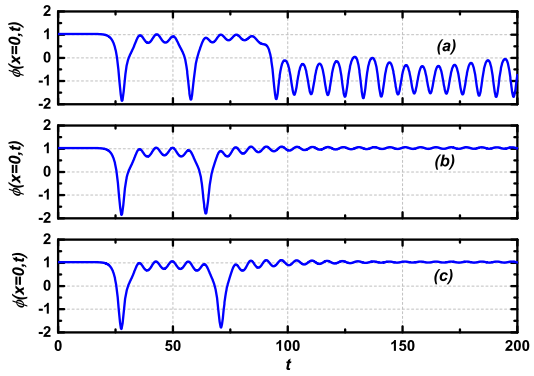

Fig. 11. Scalar field at the center of mass $\phi(0,t)$ versus time for fixed $A = 0.4$ and (a) $v_i = 0.5398$, (b) $v_i = 0.5441$ and (c) $v_i = 0.5464$.

For $A = 0.4$ (Fig. 10b) there is the formation of two more false two-bounce windows beside the zeroth-order. This is possibly connected to the presence of a maximum in the energy of the vibrational state, as seen in Fig. 7. This behavior of false windows grows with the reduction of A until a complete disappearance of two-bounce windows for $A \simeq 0.33$ (see diagram of Fig. 5). For example, Fig. 10a for $A = 0.3$ shows bion and 1-bounce scattering, despite the presence of a vibrational state. There, instead of the expected windows, we have a set of oscillations accumulating in $v = v_{crit}$. We also note that the larger is A, the larger are the widths of the two-bounce windows (compare Fig. 10b for $A = 0.4$ with Fig. 10d for $A = 0.9$).

The peaks in Figs. 10a–10d corresponding to false windows and the true two-bounce windows can be analyzed counting the number M of cycle oscillations of $\phi(0,t)$ between each collision. Each window can then be labeled by an integer $m = M - 2$ [14]. In Figs. 11a–11c we describe the behavior of $\phi(0,t)$ for case $A = 0.4$, corresponding to the diagram $t \times v_i$ of Fig. 10b. Figs. 11b and 11c show that $\phi(0,t)$ oscillates $M = 5$ and $M = 6$ times, respectively, corresponding to the expected third ($m = 3$) and fourth ($m = 4$) two-bounce windows. The first two two-bounce windows are missing. One example from the second ($m = 2$) missed two-bounce windows is seen in Fig. 11a, corresponding to the third peak of Fig. 10b. Indeed, including the first two bounces of Fig. 11a the function $\phi(0,t)$ oscillates $M = 4$ times, so the order of the peak is $m = 2$. The structure of false two-bounce windows is evident since after the second bounce $\phi(0,t)$ oscillates for a while around the vacuum ($\phi = 1$, according to Fig. 10), decaying further to the second vacuum, with the field oscillating in a bion pattern around $\phi \sim -1$.

4. Conclusions

In this work we have studied a hybrid degenerate vacua to vacuumless model depending on a parameter A. Our main findings where summarized in Fig. 5. We found that the separation of vacua has remarkable effects on the structure of two-bounce windows. It was shown that the potential of perturbations transits from a smooth valley (with one vibrational state) to a volcano shape (with no vibrational state). The interesting region is that of an intermediate value $A = 0.44$, where the energy of the vibrational state is maximum. This is close to $A_3 = 0.45$ where the structure of two-bounce windows starts to be traded by false windows.

The false two-bounce windows include kink–antikink scattering processes of a very particular aspect: the scalar field $\phi(0,t)$ shows, for a short time interval, the expected 2-bouncing behavior; however, contrary to the true two-bounce windows, and instead of later being separated, the kink–antikink pair is turned either to an oscillon or a bion state, finally resulting in total annihilation. In particular, the oscillon state seems to have a more general relation to the nonlinearity of the model, not necessarily related to the presence of either true or false two-bounce windows.

The process of trading true by false two-bounce windows grows when one reduces the parameter A to the region where the vacua are more separated. In particular the parameter $A_1 \lesssim A \lesssim A_2$, with $A_1 = 0.25$ and $A_2 = 0.34$ is characterized by the total suppression of two-bounce windows, substituted by a sequence of false two-bounce windows, despite having one vibrational state (see Fig. 10a).

In the model studied here the CSW mechanism works in the sense of predicting the pattern of two-bounce windows. However, for some values of A the mechanism is frustrated, the kink–antikink pair being not allowed to separate anymore. In some sense the model introduces an asymmetry in the influence of A on the behavior of the scattering processes: the region $A < A_3$ favors the frustration of the scattering mechanism followed by a changing of vacuum of the solutions. On the other hand, the region $A > A_3$ there is no such frustration process and the CSW works properly. This is a clear indication of the influence of the vacuumless character on the frustration of two-bounce windows.

Acknowledgements

The authors thank FAPEMA, Brazil, Grants PRONEX 01452-14, PRONEM 01852/14, universal – 01061/17, universal – 01332/17, universal – 01191/16 and CNPq, Brazil, Grant 309842/2015-8 for financial support.

References

[1] T. Dauxois, M. Peyrard, Physics of Solitons, Cambridge University Press, Cambridge, 2006.
[2] J. Khoury, B.A. Ovrut, P.J. Steinhardt, N. Turok, The ekpyrotic universe: colliding branes and the origin of the hot big bang, Phys. Rev. D 64 (2001) 123522, arXiv:hep-th/0103239.
[3] Yu-ichi Takamizu, Kei-ichi Maeda, Collision of domain walls and reheating of the brane universe, Phys. Rev. D 70 (2004) 123514.
[4] Paul M. Saffin, Anders Tranberg, Particle transfer in braneworld collisions, J. High Energy Phys. 08 (2007) 072, arXiv:0705.3606.
[5] S.W. Hawking, I.G. Moss, J.M. Stewart, Bubble collisions in the very early universe, Phys. Rev. D 26 (1982) 2681.
[6] J. Braden, J.R. Bond, L. Mersini-Houghton, Cosmic bubble and domain wall instabilities I: parametric amplification of linear fluctuations, J. Cosmol. Astropart. Phys. 03 (2015) 007, arXiv:1412.5591.
[7] Jonathan Braden, J. Richard Bond, Laura Mersini-Houghton, Cosmic bubble and domain wall instabilities II: fracturing of colliding walls, J. Cosmol. Astropart. Phys. 08 (2015) 048.
[8] Jonathan Braden, J. Richard Bond, Laura Mersini-Houghton, Cosmic bubble and domain wall instabilities III: the role of oscillons in three-dimensional bubble collisions, J. Cosmol. Astropart. Phys. 09 (2015) 004.
[9] E.B. Bogomolny'i, The stability of classical solutions, Sov. J. Nucl. Phys. 24 (1976) 449.
[10] M.K. Prasad, C.M. Sommerfield, Exact classical solution for the 't Hooft monopole and the Julia–Zee dyon, Phys. Rev. Lett. 35 (1975) 760.
[11] D. Bazeia, Defect structures in field theory, arXiv:hep-th/0507188.
[12] C.A. Wingate, Numerical search for a ϕ^4 breather mode, SIAM J. Appl. Math. 43 (1) (1983) 120–140.
[13] D.K. Campbell, J.S. Schonfeld, C.A. Wingate, Resonance structure in kink–antikink interactions in ϕ^4 theory, Physica D 9 (1983) 1.
[14] P. Anninos, S. Oliveira, R.A. Matzner, Fractal structure in the scalar $\lambda(\phi^2 - 1)^2$ theory, Phys. Rev. D 44 (1991) 1147.
[15] R.H. Goodman, R. Haberman, Kink–antikink collisions in the ϕ^4 equation: the n-bounce resonance and the separatrix map, SIAM J. Appl. Dyn. Syst. 4 (2005) 1195.
[16] P. Dorey, K. Mersh, T. Romanczukiewicz, Y. Shnir, Kink–antikink collisions in the ϕ^6 model, Phys. Rev. Lett. 107 (2011) 091602.
[17] Vakhid A. Gani, Alexander E. Kudryavtsev, Mariya A. Lizunova, Kink interactions in the $(1+1)$-dimensional ϕ^6 model, Phys. Rev. D 89 (2014) 125009.
[18] P. Ahlqvist, K. Eckerle, B. Greene, Kink collisions in curved field space, J. High Energy Phys. 04 (2015) 059.

[19] T.S. Mendonça, H.P. de Oliveira, A note about a new class of two-kinks, J. High Energy Phys. 06 (2015) 133.
[20] T.S. Mendonça, H.P. de Oliveira, The collision of two-kinks defects, J. High Energy Phys. 1509 (2015) 120.
[21] Vakhid A. Gani, Vadim Lensky, Mariya A. Lizunova, Kink excitation spectra in the $(1+1)$-dimensional ϕ^8 model, J. High Energy Phys. 08 (2015) 147.
[22] F.C. Simas, Adalto R. Gomes, K.Z. Nobrega, J.C.R.E. Oliveira, Suppression of two-bounce windows in kink–antikink collisions, J. High Energy Phys. 09 (2016) 104.
[23] Aliakbar Moradi Marjaneh, Vakhid A. Gani, Danial Saadatmand, Sergey V. Dmitriev, A. Kurosh Javidan, Multi-kink collisions in the ϕ^6 model, J. High Energy Phys. 07 (2017) 028.
[24] Patrick Dorey, Aliaksei Halavanau, James Mercer, Tomasz Romanczukiewicz, Yasha Shnir, Boundary scattering in the ϕ^4 model, J. High Energy Phys. 05 (2017) 107.
[25] I. Cho, A. Vilenkin, Vacuum defects without a vacuum, Phys. Rev. D 59 (1999), 021701 (R).
[26] I. Affleck, M. Dine, N. Seiberg, Dynamical supersymmetry breaking in supersymmetric QCD, Nucl. Phys. B 241 (1984) 493.
[27] P. Binetruy, M. Gaillard, Y.Y. Wu, Supersymmetry breaking and weakly vs. strongly coupled string theory, Phys. Lett. B 412 (1997) 288.
[28] I. Cho, A. Vilenkin, Gravitational field of vacuumless defects, Phys. Rev. D 59 (1999) 063510.
[29] D. Bazeia, Topological solitons in a vacuumless system, Phys. Rev. D 60 (1999) 067705.
[30] A. de Souza Dutra, A.C. Amaro de Faria Jr, Vacuumless kink systems from vacuum systems: an example, Phys. Rev. D 72 (2005) 087701.